RSC Advances

PAPER

View Article Online
View Journal | View Issue

Cite this: *RSC Adv.*, 2022, **12**, 13971

Insight on the effect of Ni and Ni–N co-doping on SnO_2 anode materials for lithium-ion batteries

Jianjian Shi, [a] Tao Chen,*[a] Minhang Song[b] and Xiaoli Sun*[cd]

With the increased demand for high-rate performance Li-ion batteries, it is necessary to find available methods to improve the rate properties of SnO_2 electrodes. It is noteworthy that doping was considered to be a feasible means. The electronic structures and diffusion energy barriers of Ni-doped and Ni–N co-doped SnO_2 were calculated based on density functional theory. The results estimated that the energy gaps of Ni-doped and Ni–N co-doped SnO_2 are 1.07 eV and 0.94 eV, which both are smaller than the value of 2.08 eV of SnO_2. These exhibit that the conduction properties of SnO_2 can be enhanced by doping with the Ni or Ni–N atoms. Moreover, the diffusion properties of Li can also be improved by doping with Ni–N atoms due to the diffusion energy barrier of Li from the B to C point for Ni–N co-doped SnO_2 being 0.12 eV smaller than the value of 0.24 eV for the pristine SnO_2. Meanwhile, the diffusion energy barriers of Li along other pathways for Ni–N co-doped SnO_2 are almost the same as 0.24 eV for SnO_2. These results show that both the electronic and ionic conductivity of SnO_2 can be enhanced by Ni–N co-doping, which provides a theoretical explanation to promote the rate properties of SnO_2 by Ni–N co-doping as anode materials for Li-ion batteries.

Received 21st February 2022
Accepted 2nd May 2022

DOI: 10.1039/d2ra01145j

rsc.li/rsc-advances

1. Introduction

Lithium-ion batteries (LIBs) have been extensively applied in portable electronics and are expected to be used in electric vehicles (EV) and plug-in hybrid electric vehicles (HEV). Further improvements in energy and power density put forward higher requirements on either new electrode materials or their novel structural design. In the past few decades, significant efforts have been made to meet these needs. Rutile SnO_2 has become one of the most promising substitutes for graphite anode materials owing to its high theoretical capacity (781 mA h g^{-1}) compared with the theoretical capacity (372 mA h g^{-1}) of graphite.[1–4] However, there is a severe impediment to the development of SnO_2 as anode materials for LIBs because of its poor electric conductivity. Moreover, compared with two-dimensional materials, such as black phosphorus (BP), defective graphene, Li diffusion energy barrier in the bulk SnO_2 is high.[5–8] Therefore, it is necessary to find a feasible method to improve electronic and ionic conductivities of SnO_2.

The conduction property of SnO_2-based composites with conducting materials (such as carbonaceous materials and conducting polymers) is high in comparison with SnO_2, in accordance with the quantitative experiments.[9–11] Meanwhile, other methods used to improve the rate property of SnO_2 also play an essential role. For instance, doping, the metal cationic (such as Al, Mo, Ni, Co, Cu, Sb, W) doping, non-metal anionic (such as N, P, F) doping, or metal and non-metal (such as Ni–N, Co–N, Cu–N) co-doping can also be used to enhance the electrochemical properties of SnO_2 as anode materials.[12–22] Moreover, the rate property of SnO_2 with graphene as electrode for LIBs was investigated by Miao *et al.* based on the density functional theory (DFT) method.[6] They found that the Li ionic conductivity of SnO_2 with graphene was enhanced due to a new Li diffusion path [110] with a low diffusion barrier of Li compared to the pristine SnO_2 with [001] direction.[6,7]

Although the electronic and ionic conductivities of SnO_2 as the anode material for LIBs can be enhanced with distinguishable modified techniques. However, the improvement of SnO_2 by doping with impurity atoms mainly focuses on the experiment. There are few investigations to explain why the rate property of SnO_2 improved by doping is high compared with the pure SnO_2. Therefore, herein, the electronic and ionic conductivities of SnO_2 as anode materials for LIBs were calculated using the DFT method, and the effects of doping atoms (Ni or Ni–N) on electronic and ionic conductivities of SnO_2 were investigated.

2. Simulation methodology

The DFT calculations were performed using the SIESTA (Spanish Initiative for Electronic Simulations with Thousands of Atoms) with Perdew–Burke–Ernzerhof (PBE) generalized

[a]*School of Electronic Engineering, Chengdu Technological University, Chengdu 611730, PR China. E-mail: sjjian@cdtu.edu.cn; 570560423@qq.com*

[b]*Institute of Process Engineering, Chinese Academy of Sciences, Beijing 100190, China*

[c]*Department of Energy and Power Engineering, Tsinghua University, Beijing, 100084, P. R. China. E-mail: sunxiaolideyuye@163.com*

[d]*Beijing Graphene Institute, Beijing 100095, P. R. China*

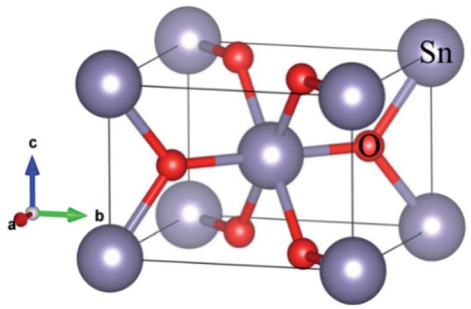

Fig. 1 The crystal structure of the bulk SnO_2, where the big and small balls are Sn and O atoms, respectively.

Table 1 Lattice parameters of the rutile SnO_2

	$a = b$ (Å)	c (Å)	Ref.
Cal.	4.734	3.220	7
	4.83	3.23	32 (PBE)
	4.815	3.225	33 (PBE)
	4.81	3.25	34 (PBE)
Exp.	4.737	3.186	25
	4.7655	3.1843	18
	4.7447	3.1870	12
	4.7467	3.1839	13
Ours	4.85	3.29	(PBE)

gradient approximation (GGA-PBE) function.[23,24] The valence electron wave functions were expanded using a DZ basis set without polarization. An energy cut-off was set to be 150 Ry. The rutile SnO_2 with $P4_2/mnm$ space group, Sn and O atoms occupy the 2a and 4f sites, respectively, using a $2 \times 2 \times 3$ k-point mesh to relax the bulk SnO_2. The relaxation of the pristine SnO_2 unit cell was performed with a conjugate gradient (CG) method until the maximum force was less than 0.02 eV $Å^{-1}$. The optimized bulk structure is shown in Fig. 1, where big and small balls are Sn and O atoms, respectively. The calculated bulk equilibrium lattice constant of SnO_2 is $a = b = 4.85$ Å, $c = 3.29$ Å, which is almost identical to the experimental and calculational values, as listed in Table 1.[12,13,18,25] A Ni occupies a Sn site (Ni-doping) and a Ni occupies a Sn site while a N replaces a O Site (Ni–N co-doping) in $2 \times 2 \times 3$ SnO_2 supercells were used to study. A $1 \times 1 \times 3$ k-point mesh to relax the Ni-doped SnO_2 and Ni–N-doped SnO_2, The Li diffusion barrier and band structure were computed after relaxing.

3. Results and discussion

The nearest neighboring heteroatom doping was only considered in our work. According to the symmetry of SnO_2, each Sn atom has 8 the nearest neighboring Sn atoms and 6 the neighboring O atoms, respectively, as shown in Fig. 1. Therefore, one Ni position doping and one Ni–N position co-doping were studied. Consider first, some materials demonstrate good computational performance but are difficult to synthesize, which limits their application in experiments or in practice.[26] So, it is important to first investigate the stability of SnO_2 in order to explore the possibility of its synthesis. We use the formation energy descriptor to measure the stability of doped SnO_2. The calculated formation energies of Ni doping and Ni–N co-doping 2.21 eV and 2.70 eV, respectively. Low formation energies of defects generally mean that these defects form easily.[27] The result indicates that Ni-doped SnO_2 and Ni–N co-doped SnO_2 are energetically favorable, which is consistent with the experimental observations.[28,29]

The conduction property of SnO_2 by doping (Ni, Ni–N-co-doping) was investigated by considering their electronic structures calculated based on the DFT. The calculated band structure and density of states (DOS) of the bulk SnO_2 are shown in Fig. 2(a) and (b), respectively. It is shown that the bulk SnO_2 is a semiconductor with a direct band gap of 2.08 eV. Its band gap is within other calculations (1.6 to 2.3 eV),[6,30,31] as shown in Fig. 2(a), where the Fermi level is zero. Fig. 2(b) shows that the energy states near the Fermi level (E_f) are mainly occupied by electrons in the 2p orbital of O atoms. The conduction band is largely contributed by 5s states of Sn atom. However, the band gaps of Ni-doped and Ni–N co-doped SnO_2 are 1.07 eV and 0.94 eV, respectively, as shown in Fig. 3(a) and (c), which both are smaller about 1 eV than that of the bulk SnO_2. Therefore, the partial transfer of electrons caused by thermal excitation from the valence band to conduction band will be more effortless in the doped SnO_2 than in the pure SnO_2.

Moreover, it can be seen from Fig. 3(b) that the E_f is localized at the maximum of the valence band (VBM) for Ni-doped SnO_2, as well as the states near E_f mainly consist of 3d states of Ni atom. For Ni–N co-doped SnO_2, as shown in Fig. 3(d), the states near E_f are occupied primarily by 3d states of Ni and 2p states of N. This indicates that the states near E_f can be changed by doped atoms (Ni, Ni–N) for the bulk SnO_2 to improve their electronic structures. Then their degree of conductivity has been enhanced by doping with Ni and Ni–N. In addition, the conductivity of Ni–N co-doped SnO_2 is a little better than that of Ni-doped SnO_2 according to their energy gaps. The Li ion property of SnO_2 as anode material for LIBs is as significant as its electronic property discussed above. Therefore, the following Li diffusion properties of SnO_2 and SnO_2 doped were studied in the light of Li diffusion energy barrier calculated with the DFT

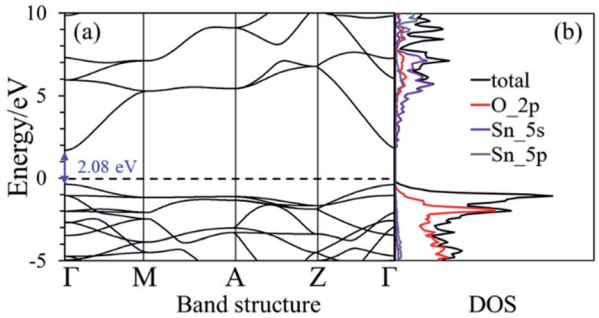

Fig. 2 (a) and (b) are the band structure and the density of state of the bulk SnO2, respectively. The dashed black line is the Fermi level that its value is zero.

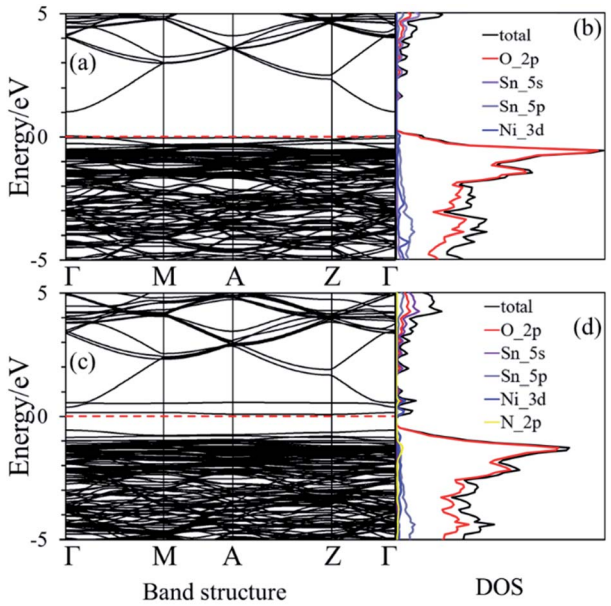

Fig. 3 (a) and (b) are the band structure and density of states of Ni-doped SnO_2, respectively. (c) and (d) are the band structure and density of states of Ni–N co-doped SnO_2, respectively. The dashed red line is the Fermi level that its value is zero.

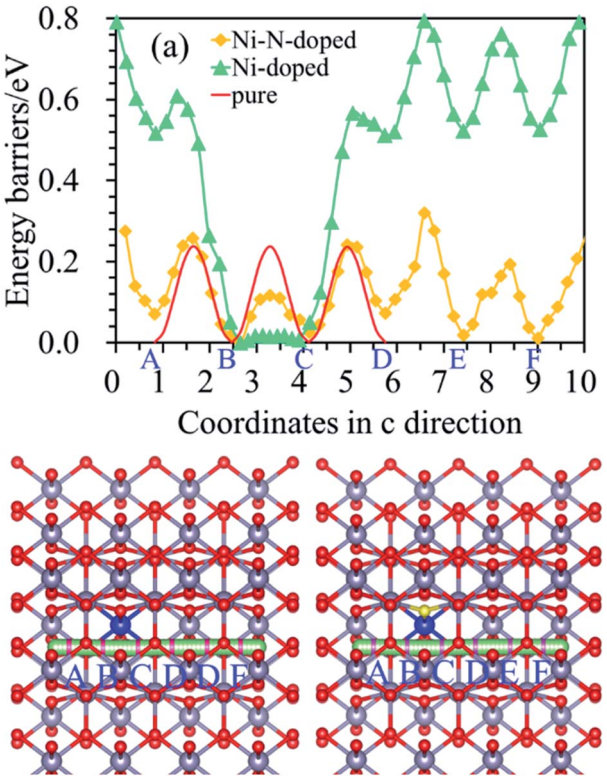

Fig. 5 (a) Energy barriers of Li, where red, green and yellow curves represent diffusion energy barriers of Li in the pure, Ni-doped, and Ni–N co-doped SnO_2, respectively. (b) and (c) show diffusion pathways of Li in the Ni-doped, and Ni–N co-doped SnO_2, respectively. Green/purple, blue, and bright yellow balls are Li, Ni and N atoms, respectively.

method. The diffusion energy barrier of Li in the bulk SnO_2 obtained is 0.24 eV, as shown in Fig. 4(a). Moreover, the diffusion path (a path from A point to D point) shown in Fig. 4(b), is identical to the experimental observation that Li diffusion direction is dominated by the [001] direction,[6,7] which both is a one-dimensional diffusion path.

The diffusion path of Li in Ni-doped SnO_2 and Ni–N co-doped SnO_2 remains one-dimensional, as shown in Fig. 5(b) and (c), but the diffusion energy is different. It can be seen from Fig. 5(a) that the energy barriers of Li for the nearest neighbor diffusion path (from B to C point) in the Ni-doped SnO_2 and Ni–N co-doped SnO_2 are 0.02 eV and 0.12 eV, which are both less than the value (0.24 eV) of the bulk SnO_2, which exhibits that the Li ionic conductivity of Ni-doped SnO_2 and Ni–N co-doped SnO_2 has been greatly improved for the nearest neighbor path. Furthermore, the energy barriers of Li far from the nearest-neighbor diffusion path (such as from C to D point, D to E point, and E to F point) be also calculated to see the effect of dopant atoms on all diffusion properties. For Ni-doped SnO_2, diffusion barriers of Li from C to D, D to E site, and E to F position, are 0.57 eV, 0.25 eV and 0.24 eV, respectively. The Li diffusion for the second nearest neighbor Li (from C to D site) is more difficult in Ni-doped SnO_2 than in the pure SnO_2. The adsorption energies of Li at C position for pure SnO_2, Ni-doped SnO_2 and Ni–N co-doped SnO_2 are −1.28 eV, −3.52 eV and −2.56 eV, respectively. The results show that lithium is energetically able to adsorb on C site for Ni-doped SnO_2, and Li diffusion barrier (from C to D site) as shown in Fig. 5(a) would increase because of a strong Li adsorption. Above results indicates that although the electronic conductivity of SnO_2 can be improved by Ni doping, the ionic conductivity was reduced when one Sn atom was replaced by one Ni atom because of a stronger Li adsorption at C site for Ni-doped SnO_2. Therefore, it is not beneficial to improve the electrochemical properties of SnO_2 as anode material for LIBs. However, for Ni–N co-doped SnO_2, the diffusion energy of Li from C to D position is 0.22 eV. It almost is the same as that of the pure SnO_2. Meanwhile, the energy barriers of Li (from B to C) just described above in the Ni–N co-doped SnO_2 are 0.12 eV.

The ionic conductivity of SnO_2 was enhanced by Ni–N co-doping. Therefore, both the electronic and ionic conductivity

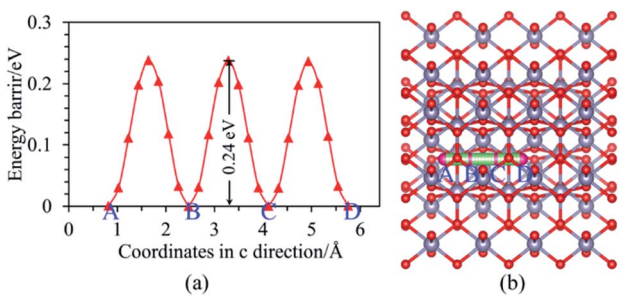

Fig. 4 (a) Energy barriers and (b) diffusion pathways of Li in the bulk SnO_2.

of SnO_2 can be improved by Ni– N co-doping. It illustrates that Ni–N co-doping in the pure SnO_2 is energetically favorable to promote the rate performance of SnO_2.

4. Conclusions

In conclusion, Ni–N co-doping in the pure SnO_2 is energetically favorable to improve both the electronic and ionic conductivity. The results calculated that the band gaps of Ni-doped and Ni–N co-doped SnO_2 are 1.07 eV and 0.94 eV, which both are smaller than the value 0.24 eV of the pure SnO_2. The diffusion energy barrier of Li from C to D for Ni-doped SnO_2 is 0.57 eV larger than the value 0.24 eV for SnO_2. However, the diffusion energy barrier of Li from B to C for Ni–N co-doped SnO_2 is 0.12 eV smaller than the value 0.24 eV for SnO_2. Meanwhile, the diffusion energy barriers of Li along pathways far from the nearest neighbor path for Ni–N co-doped SnO_2 is almost the same as 0.24 eV for SnO_2. Our results demonstrates that the electronic and ionic conductivity of SnO_2 can be promoted by Ni–N co-doping, and provides a theoretical explanation to enhance the rate property of SnO_2 by Ni–N co-doping.

Conflicts of interest

There are no conflicts to declare.

Acknowledgements

This work is supported by the Fund Project of Chengdu Technological University under Grant No. 2020RC004.

References

1 D. Guo and C. Hu, *Appl. Surf. Sci.*, 2012, **258**, 6987–6992.
2 D. W. Kim, I. S. Hwang, S. J. Kwon, H. Y. Kang, K. S. Park, Y. J. Choi, K. J. Choi and J. G. Park, *Nano Lett.*, 2007, **7**, 3041–3045.
3 J. W. Deng, C. L. Yan, L. C. Yang, S. Baunack, S. Oswald, H. Wendrock, Y. F. Mei and O. G. Schmidt, *ACS Nano*, 2013, **7**, 6948–6954.
4 Z. Lu, Z. Kong, L. Jing, T. Wang, X. Liu, A. Fu, P. Guo, Y.-G. Guo and H. Li, *Energy Fuels*, 2020, **34**, 13126–13136.
5 Q. Yao, C. Huang, Y. Yuan, Y. Liu, S. Liu, K. Deng and E. Kan, *J. Phys. Chem. C*, 2015, **119**, 6923–6928.
6 L. Miao, J. Wu, J. Jiang and P. Liang, *J. Phys. Chem. C*, 2013, **117**, 23–27.
7 F. R. Sensato, L. Gracia, A. Beltrán, J. Andrés and E. Longo, *J. Phys. Chem. C*, 2012, **116**, 16127–16137.
8 X. Fan, W. T. Zheng and J. L. Kuo, *ACS Appl. Mater. Interfaces*, 2012, **4**, 2432–2438.
9 F. Li, G. Wang, D. Zheng, X. Zhang, C. J. Abegglen, H. Qu and D. Qu, *ACS Appl. Mater. Interfaces*, 2020, **12**, 19423–19430.
10 R. Li, S. Nie, C. Miao, Y. Xin, H. Mou, G. Xu and W. Xiao, *J. Colloid Interface Sci.*, 2022, **606**, 1042–1054.
11 H. Mou, Y. Xin, C. Miao, S. Nie, S. Chen and W. Xiao, *Electrochim. Acta*, 2021, **397**, 139286.
12 C. Wei, G. Zhang, Y. Bai, D. Yan, C. Yu, N. Wan and W. Zhang, *Solid State Ionics*, 2015, **272**, 133–137.
13 X. K. Wang, Z. Q. Li, Z. W. Zhang, Q. Li, E. Y. Guo, C. X. Wang and L. W. Yin, *Nanoscale*, 2015, **7**, 3604–3613.
14 N. Wan, T. T. Zhao, S. W. Sun, Q. Wu and Y. Bai, *Electrochim. Acta*, 2014, **143**, 257–264.
15 N. Wan, P. Yu, S. Sun, Q. Wu, T. Li and Y. Bai, *Mater. Lett.*, 2014, **133**, 168–170.
16 X. Wang, X. Cao, L. Bourgeois, H. Guan, S. Chen, Y. Zhong, D.-M. Tang, H. Li, T. Zhai, L. Li, Y. Bando and D. Golberg, *Adv. Funct. Mater.*, 2012, **22**, 2682–2690.
17 X. W. Liu, D. H. Teng, T. Li, Y. H. Yu, X. H. Shao and X. P. Yang, *J. Power Sources*, 2014, **272**, 614–621.
18 N. Wan, X. Lu, Y. Wang, W. Zhang, Y. Bai, Y. S. Hu and S. Dai, *Sci. Rep.*, 2016, **6**, 18978.
19 Y. D. Wang, I. Djerdj, B. Smarsly and M. Antonietti, *Chem. Mater.*, 2009, **21**, 3202–3209.
20 Y. Feng, C. Bai, K. Wu, H. Dong, J. Ke, X. Huang, D. Xiong and M. He, *J. Alloys Compd.*, 2020, **843**, 156085.
21 A. Vázquez-López, D. Maestre, J. Ramírez-Castellanos, J. M. González-Calbet, I. Píš, S. Nappini, N. Yuca and A. Cremades, *J. Phys. Chem. C*, 2020, **124**, 18490–18501.
22 B. Liang, J. Wang, S. Zhang, X. Liang, H. Huang, D. Huang, W. Zhou and J. Guo, *Appl. Surf. Sci.*, 2020, **533**, 147447.
23 N. Troullier and J. L. Martins, *Phys. Rev. B*, 1991, **43**, 1993–2006.
24 J. P. Perdew, K. Burke and M. Ernzerhof, *Phys. Rev. Lett.*, 1996, **77**, 3865–3868.
25 J. Haines and J. M. Leger, *Phys. Rev. B*, 1997, **55**, 11144–11154.
26 Q. Sun, Q. Wang, P. Jena and Y. Kawazoe, *J. Am. Chem. Soc.*, 2005, **127**, 14582–14583.
27 J. Shi, *Int. J. Electrochem. Sci.*, 2016, **11**, 9067–9073.
28 S. S. Pan, S. Wang, Y. X. Zhang, Y. Y. Luo, F. Y. Kong, S. C. Xu, J. M. Xu and G. H. Li, *Appl. Phys. A*, 2012, **109**, 267–271.
29 S. N. Matussin, A. L. Tan, M. H. Harunsani, A. Mohammad, M. H. Cho and M. M. Khan, *Mater. Chem. Phys.*, 2020, **252**, 123293.
30 O. Mounkachi, E. Salmani, M. Lakhal, H. Ez-Zahraouy, M. Hamedoun, M. Benaissa, A. Kara, A. Ennaoui and A. Benyoussef, *Sol. Energy Mater. Sol. Cells*, 2016, **148**, 34–38.
31 W. Dong, X. Xie, J. Jia, H. Du, L. Zhong, Z. Liang and P. Han, *Electrochim. Acta*, 2014, **132**, 307–314.
32 V. Golovanov, V. Golovanova and T. T. Rantala, *J. Phys. Chem. Solids*, 2016, **89**, 15–22.
33 J. Jia, W. Zhang, Z. Liang, X. Zhang, C. Fan and P. Han, *Phys. B*, 2012, **407**, 1985–1989.
34 M. Behtash, P. H. Joo, S. Nazir and K. Yang, *J. Appl. Phys.*, 2015, **117**, 175101.